Hydrodynamic Cavitation through "Labs on a Chip": From Fundamentals to Applications

Frédéric Ayela, Wahid Cherief, Damien Colombet, Gilles Ledoux, Matteo Martini, Stéphane Mossaz, Darjan Podbevsek, Xiaoyu Qiu, Olivier Tillement

Oil & Gas Science and Technology – Rev. IFP Energies nouvelles (2017) **72**, 19

DOI: 10.2516/ogst/2017010

IFP Energies nouvelles International Conference
Rencontres Scientifiques d'IFP Energies nouvelles

Dynamics of Evolving Fluid Interfaces – DEFI Gathering Physico-Chemical and Flow Properties
Dynamiques des écoulements à interfaces fluides – au croisement de la physico-chimie et de la mécanique de fluides

Hydrodynamic Cavitation through "Labs on a Chip": From Fundamentals to Applications

Frederic Ayela[1]*, Wahid Cherief[1], Damien Colombet[1], Gilles Ledoux[2], Mateo Martini[2], Stephane Mossaz[1], Darjan Podbevsek[2], Xiaoyu Qiu[1] and Olivier Tillement[2]

[1] *LEGI, Université Grenoble Alpes, CS 40700, 38058 Grenoble Cedex 9 - France*
[2] *ILM, Université C. Bernard Lyon 1, 69622 Villeurbanne Cedex - France*
e-mail: frederic.ayela@legi.cnrs.fr

* Corresponding author

Abstract *— Monitoring hydrodynamic cavitation of liquids through "labs on a chip" (i.e. microchannels with a shrinkage, such as microdiaphragms or microventuris) is an improvement in experimental approaches devoted to study the mechanisms involved in these multiphase flows. The small sizes of the reactors do not require big substructures. Flow rates of around 1 L/h make possible the characterisation of rare, toxic or expensive pure fluids or mixtures. Moreover, because of that microfluidic approach, an unique inception of the cavitation from a laminar flow regime is also possible, that provides precious databases for simulation or modelisation. Lastly, "labs on a chip" are an extremely versatile solution to perform novel experiments, as they are embeddable in tools basically designed to proceed with small samples (confocal microscopy, spectroscopy). We present here a summary of the former experiments performed by our team, concerning the fundamental aspects of hydrodynamic cavitation in a microchannel. We have recorded, with thermosensitive nanoparticles dispersed in water, the thermal signature of the growth and collapse of bubbles. We were also able to monitor the cavitation flow regime from a laminar single liquid phase. We are currently involved in applicative studies of hydrodynamic cavitation in microchannels, and preliminary results concerning liquid phase exfoliation of graphene will be also presented.*

Résumé — Cavitation hydrodynamique "sur puce" : Aspects fondamentaux et appliqués — L'émergence de la cavitation hydrodynamique 'sur puce' (cavitation dans des microcanaux comportant une réduction localisée de leur section de passage) est un atout pour l'étude des mécanismes impliqués dans ce type d'écoulements diphasiques. Les dimensions réduites des réacteurs s'affranchissent de l'utilisation d'infrastructures lourdes. Des débits de l'ordre du litre par heure rendent possible l'étude de fluides rares, toxiques ou coûteux, ainsi que l'étude de mélanges. De plus, cette approche microfluidique est la seule qui permet sous certaines conditions l'apparition de la cavitation à partir d'un régime d'écoulement laminaire, ce qui fournit des données expérimentales intéressantes pour la modélisation. Enfin, la dimension réduite des "laboratoires sur puce" leur permet de s'intégrer dans des schémas expérimentaux (microscopes confocaux, spectrométrie) inenvisageables à plus grande échelle. Nous présentons ici un récapitulatif de résultats récemment obtenus par notre équipe, concernant des aspects fondamentaux et appliqués au génie des procédés de la cavitation hydrodynamique sur puce. Nous avons pu détecter la signature thermique de l'évaporation et de la condensation de bulles, grâce à des nanoparticules thermofluorescentes dispersées dans l'écoulement. Nous avons également piloté la transition vers la cavitation à partir d'un écoulement laminaire. Nous présentons enfin les premiers résultats de nos travaux en cours, concernant l'exfoliation en phase liquide du graphène assistée par microcavitation.

INTRODUCTION

Cavitation refers to the growth and collapse of vapour bubbles inside a liquid whose static pressure is submitted to transitions below and above the vapour pressure. Ultrasounds of sufficient intensity can create acoustic cavitation in a vessel of limited size. For its part, hydrodynamic cavitation results from the Bernoulli law: a constriction of the section of the flow will increase the velocity of a single liquid phase fluid. When the resulting decrease of the static pressure falls below the vapour pressure P_{vap}, it should trigger the inception of cavitation. Downstream, an expansion of the section of the flow slows down the velocity, and bubbles collapse because of the recovery of the static pressure. For both kinds of cavitation, bubbles may be considered as microreactors, because of the physico-chemical effects associated to the violent collapse [1] (maximum temperature and pressure inside the bubble $T_{max} \approx 10^4$ K and $P_{max} \approx 10^3$ bar).

High and low frequency ultrasounds are widely used in liquids for applications such as SonoChemistry (SC) or MultiBubbles SonoLuminescence (MBSL). For its part, hydrodynamic cavitation is generally associated to negative consequences of erosion, that occurs on the walls of the channel downstream the constriction. Erosion is the consequence of repeated shock waves and/or liquid microjets emitted after the collapse of the bubbles. The relative low amount of publications concerning SC or MBSL observed in hydrodynamic cavitation may be explained by a number of reasons, among others the macroscopic size of the channels. Bubbles in an acoustic wave are submitted to several cycles, whereas the effective number of cycles suffered by a bubble in a macroscopic cavitating flow is lower. And some special liquids or blends cannot be easily tested with macroscopic tools.

Microfluidics offer unique opportunities to perform smart experiments unachievable at macroscale. An idea, which is largely admitted, is that microfluidics is required when a small amount of fluid is needed. That is true and may be helpful when dealing with rare or toxic liquids. However, it must be pointed out that a parallel arrangement of submillimeter channels micromachined onto a silicon substrate may deliver flow rates of several liters per hour. Another asset of microfluidics is that because of small hydraulic diameters d_H involved, laminar and turbulent flow regimes may be controlled and monitored, together with a very high shear rate. Moreover, it must be noticed that microchannels may be integrated in physical or optical set up (confocal microscope, etc.) unachievable for macroscopic channels. Finally, microchannels may be used as elementary bricks involved in a more general process. The possibility to perform hydrodynamic cavitation inside such microdevices is an exciting challenge.

Hydrodynamic cavitation "on a chip" is a recent technology, that could be relevant in order to scrutinize new trends relative to fundamentals or applications of cavitation. Following the initial work of Mishra and Peles [2, 3], some researchers have considered the chemical aspects of cavitation when it occurs in microfluidic systems. Fernandez Rivas *et al*. [4] have enhanced the chemiluminescence of luminol by focusing acoustic cavitation inside micromachined crevices of micrometer sizes. SC of luminol and sonoluminescence of water have been reported by Tandiono *et al.* inside PolyDiMethylSiloxane (PDMS) microchannels submitted to acoustic waves [5]. To our knowledge, only one publication has investigated correlations between chemistry and hydrodynamic cavitation in microchannels and millichannels [6]. The authors have recorded an oxidation rate of potassium iodide up to 60 nm/min at a flow rate of ≈5 L/h in a millichannel, but no measurable reaction has been observed in microchannels. They believed that by decreasing the constriction size, one decreases the pressure recovery time and one increases the strength of the bubble collapse. But the growing time of the bubbles is also reduced. An optimum configuration has to be found and further experiments are needed for a better knowledge of the real phenomenon involved.

For the past five years, our team has developed a large number of experiments devoted to "cavitation on a chip". That paper summarises some important conclusions obtained, and gives the most recent results of our currently managed researches.

1 MICROSYSTEMS DESIGNED FOR HYDRODYNAMIC CAVITATION

1.1 Geometries and Machining

The microchannels are machined onto polished silicon wafers. Silicon is a well suited material for the etching processes involved in micromachining.

Hydrodynamic cavitation results from a local constriction of the cross section of the flow. Microdiaphragms and microventuris were the only geometries considered up to now to perform hydrodynamic cavitation "on a chip" [2, 3, 7]. We have recently developed a new geometry, so-called microstep profile, which will be presented in Section 3. A general scheme of the evolution of the static pressure along the flow for the diaphragm and venturi profiles is represented in Figure 1. The design of the sizes of the channels and of their related constriction is monitored by considerations taking into account a balance between the pressure losses due to the shrinkage and the dynamic pressure drop $1/2\rho u_0^2$, where ρ is the density of the liquid and u_0 the average velocity in the constriction (the dynamic

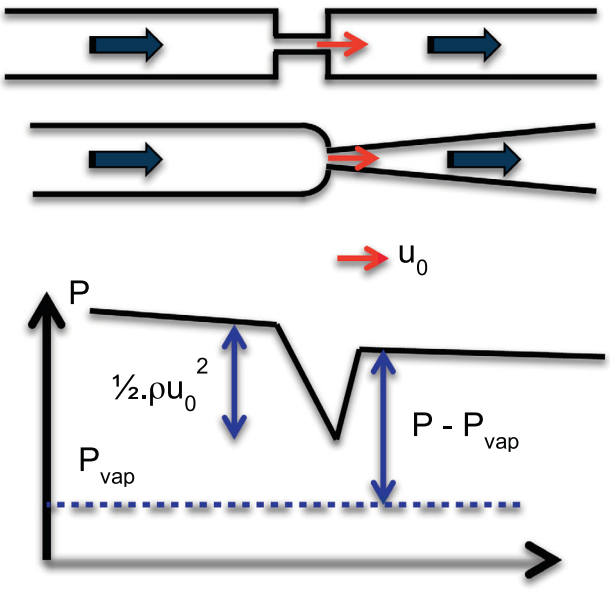

Figure 1

Top view of two geometries of microchannels considered for hydrodynamic experiments, and the corresponding pressure line. The pressure line obeys the Bernoulli principle. When a sufficiently high velocity is reached in the constriction, the pressure falls below P_{vap} and bubbles can growth. Downstream, the velocity decreases and the pressure recovers a higher value.

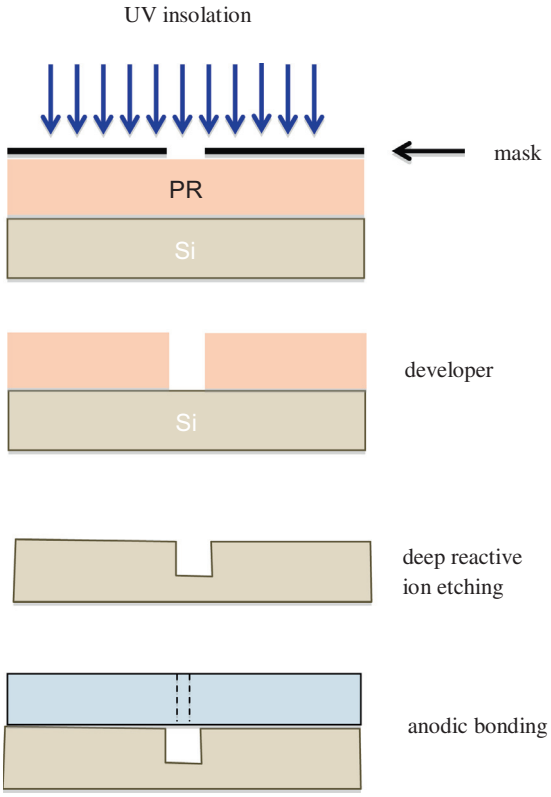

Figure 2

Experimental steps involved in the micromachining of cavitating labs on a chip. Details are given in the text.

pressure upstream and downstream the constriction is negligible in front of $1/2\rho u_0^2$).

Detailed calculations [7] demonstrate that in microdiaphragms and microventuris, the width w of the constriction must be shorter than the height H of the grooved channel. The vertical walls of the channels must be performed by a so-called Deep-Reactive Ion Etching (D-RIE) process.

Details on micromachining processes for microfluidics are readily available in the literature [8]. A general scheme of the experimental steps involved in the micromachining of the channels is described in Figure 2. A thin UltraViolet (UV) sensitive photoresist layer (≈3 µm) is spin coated onto the wafer. The wafer is baked at 100 °C for 1 min, and then covered by a mask that is non-transparent except in the area that will be subsequently etched. An UV irradiation (≈20 mJ/cm^2) is applied to the exposed photoresist. A developer solution removes the irradiated resist and reveals the top-view of the channel. A D-RIE process allows an anisotropic etching of the substrate, and a channel of uniform depth is produced.

The last step is the packaging with a hermetic encapsulation. A Pyrex cap is anodically bonded onto the silicon channel. Anodic bonding is performed at atmospheric pressure on a hot plate at 400 °C, by applying a negative tension (−500 V) to the Pyrex cap in order to neutralize positive ions present in Pyrex glass and to create an electrostatic bond at the interface with silicon. Prior to bonding, the Pyrex cap is drilled to provide the fluidic connection.

Typical heights of the channels range from $H = 120$ µm to $H = 140$ µm. The total length of the channel is around 5 mm. The width of the throat of the microventuris is typically 30 µm $< w <$ 50 µm, the angle of the diffuser is ≈4°. Concerning the microdiaphragms, the width of the shrinkage 50 µm $< w <$ 80 µm and the width of the channel $W = 500$ µm. Scanning Electron Microscope (SEM) snapshots of the throttle of a microventuri and of a cross-sectional view of a microdiaphragm are displayed in Figure 3.

1.2 Hydrodynamic Behaviour

The hydrodynamic behaviour of the devices is characterised by a $\Delta P(Q)$ plot, where ΔP is the total pressure drop applied to the device and Q is the flow rate. The singular pressure loss in the constriction is generally predominant, and the relationship obeys $\Delta P \approx Q^2$. Experimental runs consist in increasing step by step the pressure drop and in recording the corresponding flow rate. Above a critical flow rate Q_{cav} that depends on geometrical parameters, cavitation

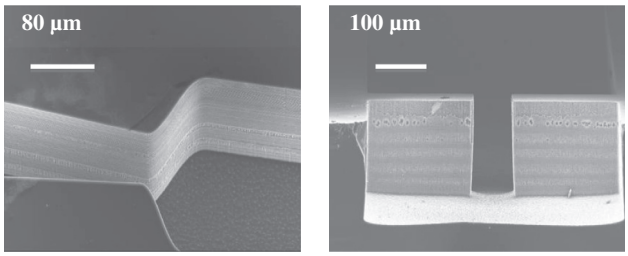

Figure 3

a) SEM snapshots of the throttle of a micro venturi and of the b) cross-sectional view of a sacrificed microdiaphragm sample micromachined in a silicon wafer.

is likely to occur. With microdiaphragms or microventuris considered here, 0.3 L/h < Q_{cav} < 1 L/h with pressure drops below 8 bar. Metastable effects have been observed with pure deionized water as the working fluid, because the smooth walls of the micromachined devices prohibit the contribution of the nuclei [7]. Once the two-phase cavitating flow has started, there is a small drop of the flow rate together with a low but audible crackle due to the collapse of the bubbles. To characterise the strength of the hydrodynamic cavitation, a cavitation number σ is generally used:

$$\sigma = \frac{P_{out} - P_{vap}}{\frac{1}{2}\rho u_0^2} \quad (1)$$

where P_{out} is the static pressure at the outlet of the channel.

A geometric meaning of σ can be understood from Figure 1. $\sigma < \sigma_{cav}$ (σ_{cav} being the cavitation number calculated with the theoretical critical flow rate Q_{cav}) means that cavitation is possible. Because of the singular pressure loss due to the constriction, $\sigma_{cav} < 1$. The smallest σ, the strongest cavitating flow regime.

Microventuris give way to pocket cavitation: a vapour pocket is linked to the throat and develop on one side of the diffuser downstream [9]. Microdiaphragms give way to shear cavitation: the liquid jet emerging from the constriction shears a residual liquid pocket, inducing vortices from where bubbles clouds can grow up.

2 FUNDAMENTAL STUDIES

We present here an overview of two fundamental studies where microdiaphragms and microventuris are at the origin of cavitation. The first one has exhibited for the first time thermal effects of water around the cavitation area. The second one was devoted to the cavitation of alcohols and binary mixtures, and an anomalous effect of ethanol has been confirmed.

2.1 Experimental Evidence of Thermal Effects

Cavitation is defined as the phenomenon of formation of vapour bubbles in a liquid, in a region where the pressure of the liquid falls below its vapour pressure. Vapour production extracts latent heat L_{vap} from the liquid surrounding the bubbling cloud. As a consequence, a cooling of the liquid around the gaseous cavity is expected. Inversely, the collapse of the bubbles, once the pressure has recovered a value above the saturation, is expected to heat the liquid. That is usually named as the thermal effects in cavitation [10]. In a cavitating flow, cooling and heating at the bubbling interfaces occur in separate areas. Some important applications are concerned by thermal effects. In the spatial industry with the design of cryogenic space rocket engines propellers and inducers, thermal effects have a positive consequence since the cooling of the liquid takes it away from the saturation line. In high pressure diesel direct injection nozzles, where cavitation is likely to occur, that may affect the fuel atomisation and indirectly the combustion yield [11, 12]. In process engineering as SC where OH° radicals produced inside a collapsed bubble diffuse in the surrounding liquid, a better knowledge of the thermal effects should be welcome.

The typical temperature difference ΔT obeys $\Delta T = B\Delta T°$ with $\Delta T° = \rho_v L_{vap}/\rho_l c_l$ where ρ_v and ρ_l are the density of the vapour and liquid phase respectively, and c_l is the specific heat of the liquid. The value of B results from the choice of a global model, and it is obvious that an experimental determination of ΔT will endorse the suitable model. $\Delta T°$ = 0.01 K for water as the working fluid; $\Delta T°$ = 0.94 K for isopropanol. The thermal effects have never been directly recorded at macroscale, because measurements are not obvious in an unstationary turbulent flow.

Hydrodynamic cavitation in microchannels has allowed us to make a decisive step towards a better analysis of thermal effects in water [13, 14]. The principle of the experiment may be summarised as follows. To perform local temperature measurements in the liquid phase of a cavitating microflow, hydrophilic thermofluorescent nanoparticles were dispersed in deionized water. When submitted to a laser irradiation, the functionalized nanoparticles emit a two-peak spectrum at higher wavelengths. One peak is temperature sensitive, the other not. After calibration, the ratio of the amplitude of the two emitted peaks gives the temperature of the nanoparticle, which is the temperature of the surrounding liquid owing to the low specific heat of each nanoparticle. Moreover, the signal is free from any perturbation and fluctuation from the exciting laser wave. With such a metrology, we could take advantage of the reduced size and volume of the microchannel, because the thermal mapping was proceeded with a confocal microscope. The channel under test was set on a 3D piezoelectric holder. The laser was focused on a voxel of a few micrometer in size. The total intensity emitted

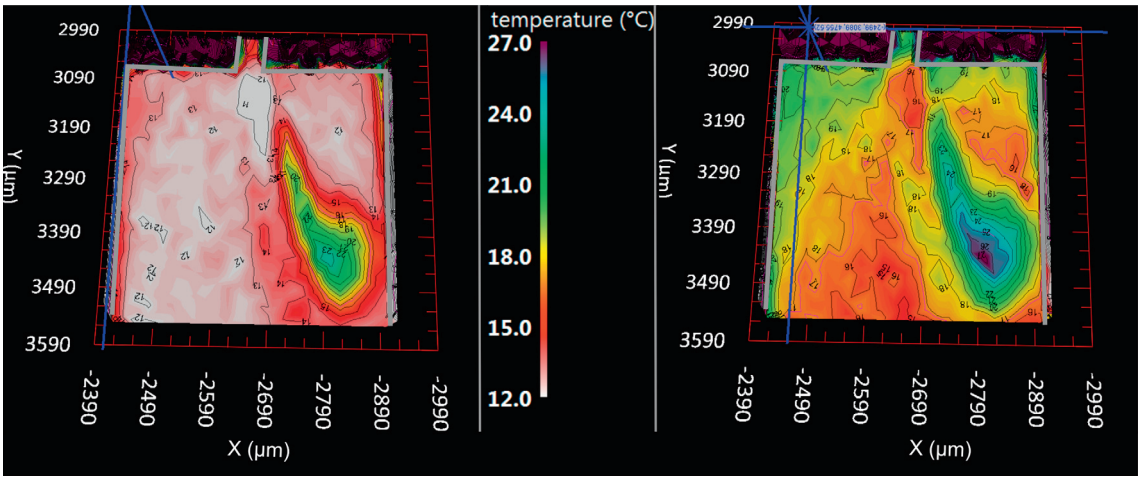

Figure 4

Thermal mapping of the liquid phase of a cavitating flow downstream a microdiaphragm, recorded in layers located at: a) z = 98 µm and b) z = 114 µm from the bottom of the channel 124 µm in height. The colour – temperature code is inserted in the figure. The border of the channel is partly underlined in Figure 4a for a better understanding.

by thermofluorescent nanoparticles traveling through a voxel is also an indication of the void fraction, because the nanoparticles are hydrophilic and are supposed lie in the liquid phase of the two-phase flow. By scanning in the three directions of space, the whole microflow could be scrutinized in around 20 min. The main disadvantage of this experimental set up is that steady state flows must be reached. It is possible to record unstationary events, but limited over one fixed voxel.

Results recorded with a microdiaphragm of hydraulic diameter d_H = 77 µm and height H = 124 µm have been published recently [13, 14]. In such sheared flows, cavitation is induced by vortices downstream the constriction. The emerging liquid jet is deflected towards the upper left side of the flow.

Two typical pictures are reported here (Fig. 4a and 4b). Figure 4a exhibits a cooling of the water of about –3 K, at a distance z = 98 µm from the bottom of the channel. The cooling arise just downstream the constriction and should correspond to the heat extracted from the surrounding liquid to provide the evaporation. Figure 4b exhibits a straight heating (+10 K over a distance of ≈100 µm), at a distance z = 114 µm from the bottom of the channel. That heating is observed where bubbles collapse and should correspond to the consequence of condensation of the bubbles on the surrounding liquid. However, other explanations may be still considered, as for example viscous effects enhanced by the thermal isolation from the vapour. Further experiments are in progress on other microdiaphragms, and on microventuris, with water as the working fluid. The following step will consider nanofluids with another base liquid having a $\Delta T°$ different to that of water. We believe that at the end of these measurement series, the collected data will provide information sound enough to confirm the role of thermal effects.

2.2 Hydrodynamic Cavitation of Binary Mixtures and the Anomalous Behaviour of Ethanol

The study of hydrodynamic cavitation of blends is relevant, in regards of the consequences in ignition engines. For these applications, the consequences of alcohol and ether addition are increasingly studied [15, 16]. Cavitation is also likely to enhance spray atomization inside diesel injection nozzles [11, 12].

We have studied three binary liquid mixtures: water – isopropanol, DiEthyl Ether (DEE) – ethanol, DEE – 2-butanol. The inception and desinence of cavitation of these mixtures were studied through microdiaphragms and microventuris.

Some physico-chemical properties of these fluids, at ambient temperature, are listed in Table 1.

The selected fluids offer the opportunity to cover a large range of Reynolds number Re and cavitation numbers σ. Re is calculated in the constriction area. $Re = \rho u_0 d_H/\mu$ where μ is the dynamic viscosity of the liquid. The small hydraulic diameter afferent to constricted microchannels is a unique situation to make cavitation possible from an initial laminar single phase flow. It can be demonstrated that the condition $\sigma < 1$ corresponds to $d_H < \mu_l Re/(2\rho_l P_{atm})^{1/2}$. For a relatively viscous liquid as 2-butanol, $Re < 2000$ corresponds to $d_H < 630$ µm. In addition, the low viscosity of DEE is in the way of high Re numbers. The flow can then induce local

TABLE 1
Physico-chemical properties of fluids.

Fluid	M (g/mole)	ρ_1 (kg/m^3)	μ_1 (mPa s)	P_{vap} (mbar)	Γ tension (N/m)
Isopropanol	60	787	2.28	44.5	0.023
Ethanol	46	792	1.16	58.9	0.024
DEE	74	714	0.23	588	0.017
2-Butanol	74	809	4	17.4	0.025
Water	18	998	1	23	0.073

low pressure vortices, even if $\sigma > 1$. Pure liquids have been first considered [17]. Experimental results recorded with two different microdiaphragms (H = 148 µm, d_H = 95 µm, and H = 187 µm, d_H = 87 µm respectively) are plotted in Figure 5, where a dimensionless cavitation number is plotted as a function of Re. $\sigma/\sigma_{cav} < 1$ means that the global static pressure in the constriction has fallen below P_{vap}. $Re > 3000$ is characterising the establishment of a turbulent flow regime in the constriction. Empty symbols correspond to single liquid phase flows. Filled symbols correspond to two-phase flows.

Data recorded with 2-butanol and isopropanol were the first ever published experimental evidences of a transition from a laminar liquid single phase flow towards a cavitating one [17]. The onset of cavitation is perfectly monitored by the drop of the pressure, as a consequence of the Bernoulli law. Alternatively, it is obvious that the cavitation of DEE is due to a turbulent flow regime in the constriction. The special feature of water resides in the fact that the two-phase flow transition occurs nearby $\sigma/\sigma_{cav} < 1$ and $Re > 2000$. Here, cavitation must be the consequence of both global pressure drop and local vortices. But what is more puzzling is the behaviour of ethanol. By increasing the flow rate and Re number from the single liquid phase, the transition occurs always early when ethanol flows through microdiaphragms. The inception arises systematically at Re = 1000 and $\sigma = 2\sigma_{cav}$. Such an anomalous behaviour had been previously observed by Singh and Peles [18]. The authors had explained this early transition by considerations about the surface tension Γ of the fluid. As the true condition for a bubble of radius R to growth by evaporation of the liquid interface is $P < P_{vap} - \Gamma/R$, it was believed that the inception of cavitation for ethanol (Γ = 24 mJ/m^2) should occur prior to that of water (Γ = 73 mJ/m^2). That argument is inferred by our experiments performed with butanol (Γ = 25 mJ/m^2) and isopropanol (Γ = 23 mJ/m^2). The surface tension of these fluids is similar to the surface tension of ethanol, and no anomalous behaviour has been recorded with these latter fluids. Moreover, experiments performed with microventuris (w = 50 µm, H = 156 µm, and w = 37 µm, H = 161 µm, diffusion angles 3.5° and 4.5° respectively) did not confirm the anomalous effect observed through the diaphragms. We may conclude that it results from the intrinsic physico-chemical properties of the fluid and from the shrinkage geometry where shear effects are predominent. That point is a current open question that necessitates still a probing work.

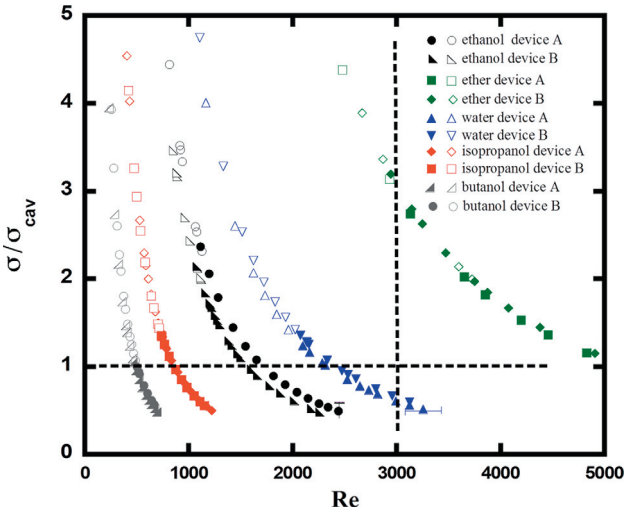

Figure 5

Normalised cavitation number plotted as a function of Re number for pure liquid flowing through microdiaphragms. Empty symbols correspond to single liquid phase data, filled symbols correspond to cavitating flows. Device A refers to d_H = 95 µm and device B refers to d_H = 87 µm.

Cavitation of three binary mixtures has been considered. The mixture DEE – ethanol has been selected in order to know if an anomalous effect was still noticeable when ethanol was present in a mixture. The mixture DEE – 2-butanol has been selected because both components had demonstrated different types of transition, when considered separately. The mixture water – isopropanol was selected because the dynamic viscosity of that mixture is very sensitive to the amount of each component. The value of the dynamic viscosity influences Re values and so the flow regime

(laminar or turbulent) present at the onset of cavitation. The viscosity and the pressure vapour of the blends were experimentally determined [17]. Each mixture was characterised at three different weight percentages. The whole results have just been published elsewhere [17], and we recall here only the main results.

Concerning the water – isopropanol mixture, it has been observed that a small amount of isopropanol lead to a dramatic increase of the viscosity. The critical flow rate above which the onset of cavitation is likely to occur is not affected by the composition of the mixture, because the vapour pressure of the blends holds a quasi constant value. As a consequence the corresponding *Re* number, which was around 2500 for pure water, shifts below $Re = 1000$ as soon as 20% in weight of isopropanol is added.

Mixtures of DEE – 2-butanol combine on the one hand a relatively viscous and low pressure vapour liquid (2-butanol) which cavitate from a laminar flow regime, and on the other hand a volatile fluid (DEE) owing a weaker viscosity. Concerning experiments with microdiaphragms, the transitions occurred early at $\sigma = 2\sigma_{cav}$ although *Re* remained below 2000. Moreover the experiments performed with these mixtures but through microventuris have exhibited an expected inception of cavitation at $Re < 2000$ and $\sigma = \sigma_{cav}$. These differences may be caused by an effect of the geometry of the constriction. The cavitation numbers seem to be overpredicted when shear cavitation takes place downstream the microdiaphragms. For these devices, conventional results (onset at $\sigma = \sigma_{cav}$) are found, but only when considering P_{vap}(DEE) instead P_{vap}(mixture). A possible explanation should be that vortices downstream the diaphragm could modify the homogeneity of the mixture composition. The presence of DEE appears to boost shear type cavitation, and the presence of 2-butanol allows to shift the inception of cavitation to lower Reynolds numbers.

Concerning ethanol – DEE mixtures flowing through microdiaphragms, an early transition occurs at $\sigma = 2\sigma_{cav}$ and $Re = 2280$ for the 20%-80% mixture. One may consider that turbulence is at the origin of the transition as it was the case for pure DEE. Ethanol – DEE mixtures with other proportions (50%, 80% ethanol respectively) display a transition from a laminar flow regime but at $\sigma/\sigma_{cav} = 1.2$. That means that by increasing the pressure drop, the experimental flow rate at which the cavitation occurs is below what is expected, even if that early transition is less marked than with pure ethanol. It seems that an anomalous effect due to ethanol is still noticeable, but slightly balanced by the presence of DEE in the mixture. Unlike the DEE – butanol blends, DEE does not prevail alone in the onset of cavitation. When these blends were tested through microventuris, the transitions occurred in a laminar flow at the expected flow rate ($\sigma \approx \sigma_{cav}$). The role of the geometry of the constriction is still obvious.

3 APPLICATION TO LIQUID PHASE EXFOLIATION

3.1 Liquid Phase Exfoliation of 2D Materials

Since the isolation and characterisation of graphene from graphite by Novoselov *et al*. more than 10 years ago [19], the research activity devoted to Two-Dimensional (2D) materials has increasingly raised up. 2D materials are substances consisting of a single layer of atoms or of a few layer sheets. Graphene, which is a single layer of graphite, is the best known among 2D materials, owing to its attractive properties such as very high electrical and thermal conductivities, or very high Young modulus. Mass production of few layer graphenes has become an exciting challenge. Beyond graphene, new 2D materials such as Transition Metal DiChalcogenides (TMDC) appear to be promising nanostructures. TMDC are crystals of the type MX_2 where M is a transition metal (Mo, W) and X is a chalcogenide (S, Se, Te). Both graphite and TMDC are lamellar crystals made of layers coupled by Van der Waals forces only. Unsurpassed mechanical, electrical, thermal and optical properties can result when these layered solids are realized as 2D materials [20]. More recently, attention has been paid to Van der Waals heterostructures, combining highly conductive graphene and optically active TMDC [21].

Two approaches lead to the production of 2D materials: the bottom-up approach (chemical vapour deposition) and the top-down approach (exfoliation). Mechanical exfoliation allowed the first production of graphene. Nowadays, Liquid Phase Exfoliation (LPE) is considered as one of the most promising process for production of monolayers and sheets on a large scale, and it is a green process [22, 23]. LPE is efficient for graphene and TMDC production, owing to the relative low intensity of the Van der Waals bonding energy. The choice of the solvents or of the surfactant (when particles are dispersed in water) is crucial: once exfoliated, a rearrangement of layers into bigger stacks has to be avoided (Fig. 6).

LPE strategies used up to now to produce graphene are:

- sonication: the solution under test is submitted to strong acoustic waves. Exfoliation is then the consequence of the force exerted to the particles by shock waves and/or liquid jet, consecutively to the collapse of the bubbles. The growth of vapour bubbles anchored between two layers may help the dissociation. However, the growth and the violent collapse of vapour bubbles are also leading to fragmentation of flakes rather than exfoliation. The roughness of the process is likely to damage the monolayers, and the quantity of the processed fluid is limited. The sonication technique is limited to low volumes, and the yield of production does not exceed 1 mg/mL after 100 h of sonication [24];
- shear process: some authors have produced graphene by shearing a graphite solution with a commercial mixer,

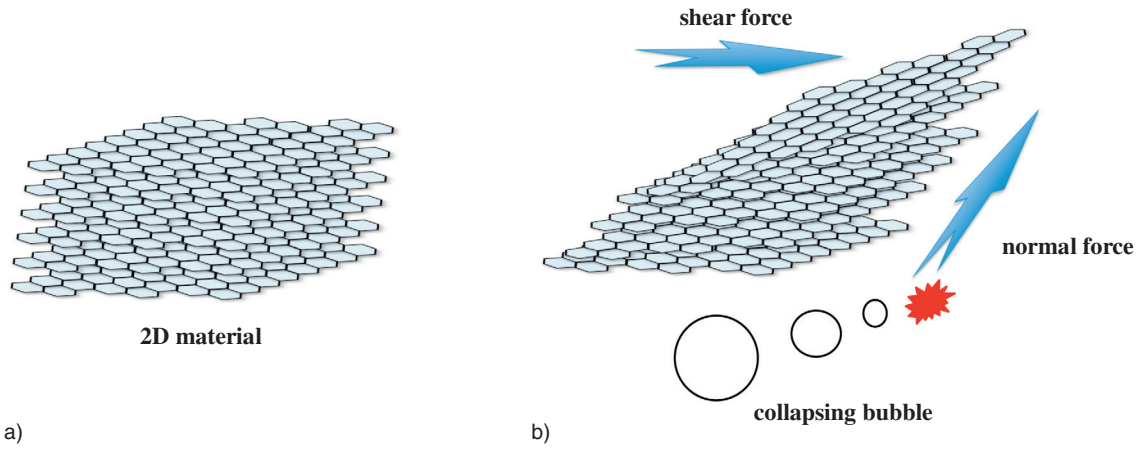

Figure 6

Scheme of liquid phase exfoliation of graphite layers a) assisted by hydrodynamic cavitation b). The exfoliation is created by shearing forces (parallel to the layers) and by normal forces (liquid jet impact, shock waves) caused by collapsing bubbles.

or by submitting a solution to centrifugal forces [25]. A turbulent flow is not necessarily required to exfoliate. This also leads to some fragmentation of the graphene. Shear rates of 10^4 s^{-1} are claimed to be sufficient, as long as the solvent surface energy is close to that of graphite [25]. Shear mixing can produce few layer graphene at a yield of approximately 5 g/h and with an average number of seven layers/flake, but with a lateral size limited to 300-800 nm;

– high pressure homogenizers produce high velocity flows through narrow orifices. High pressures above 200 bar are required. In such conditions, hydrodynamic cavitation is also likely to occur. As for sonication, cavitation can help the exfoliation but also reduce the lateral sizes of graphene layers [26, 27]. Recently [23], some authors have used high pressure homogenizers in a laminar flow regime. Exfoliation is then only caused by shear stress parallel to the layers. Higher aspect ratios of graphene layers are reached.

3.2 New Microreactors

Microchannels are ideal devices to reach high shear rates flows [28], under moderate pressure drops. Hydrodynamic cavitation "on a chip" offers the opportunity to scale down and to resume into one single device the different geometries involved with the high pressure homogenizers. With "labs on a chip", the related role of laminar, turbulent and cavitating flows can be enhanced and characterised.

Conventional cavitating microreactors such as those presented in Sections 1 and 2 (diaphragms and venturis) are not suited for that application, because the presence of solid microparticles in the flow should give way to clogging. For that application, the design of new microreactors with higher hydraulic diameters was needed. We have machined new microchannels obeying a so-called "microstep" profile.

The microstep geometry does not require vertical walls to induce cavitation, so that deep RIE reactors are not needed for the machining. The channels are machined from nitride coated silicon wafers (Fig. 7). A brief plasma etching of the Si_3N_4 nitride layer uncovers the silicon that is then etched in a 80 °C KOH solution (etch rate ≈ 60 µm/h). The residual nitride layer is then acting as a mask, because the etch rate of Si_3N_4 in KOH is negligible. A second lithography removes the nitride remaining between the two cavities. Continuing the KOH etching leads to the requested microstep profile. Owing to the crystalline orientation of silicon, the walls are not vertical but oriented at 54° from the horizontal plane.

The channels have a larger width (1 or 2 mm) and the gap h between the top of the step and the Pyrex cap is ≈110 µm. A SEM snapshot of the silicon part of a microchannel is displayed in Figure 8.

The inception of cavitation arises easily when the ratio of the height h of the gap to the total height H of the channel is below 0.4. That occurs under the same range of pressure drop that with microdiaphragms or microventuris, but at higher flow rates (≈10 L/h).

3.3 Preliminary Results on Graphene Exfoliation

Two preliminary tests have been performed on graphite dispersions in an aqueous surfactant (sodium cholate, NaC) solution. Some parameters have been modified from the first to the second test: the initial size and the concentration of the particles; the cavitation number σ of the flow and the microreactor; the duration of the process; the centrifugation rate of the solution before analysis. The process conducted

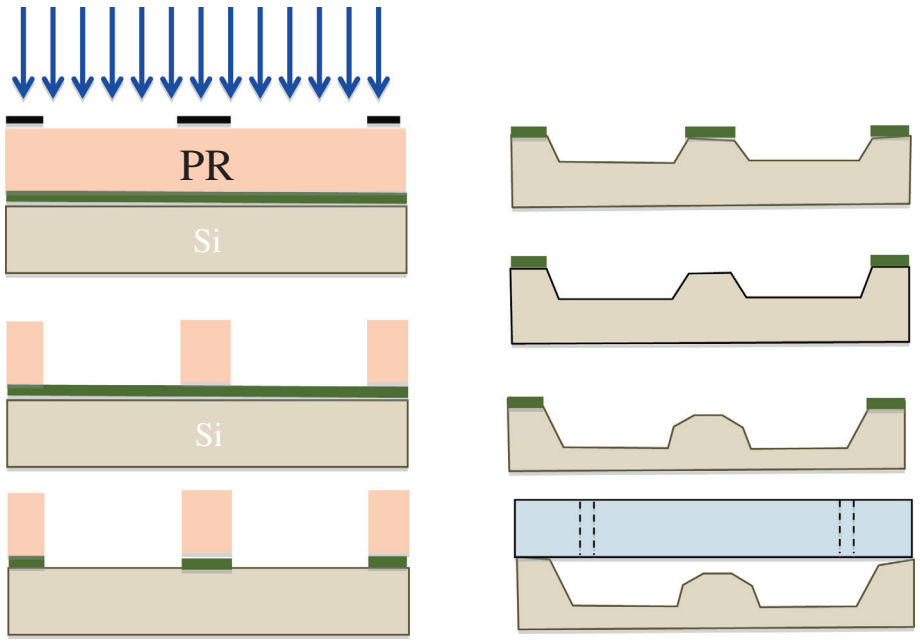

Figure 7

Experimental steps involved in the micromachining of a so-called microstep cavitating lab on a chip.

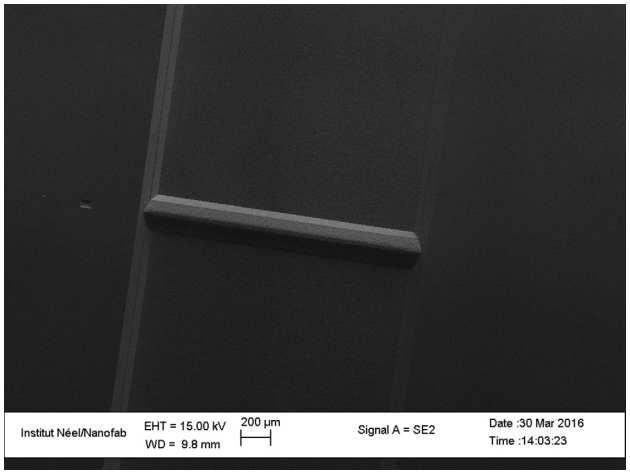

Figure 8

SEM snapshot (top view) of the silicon part of a microstep channel before anodic bonding.

with the two batches of graphite dispersions, noted A and B, is summarised in Table 2.

The test presented in column A concerns small particles submitted to a relatively short duration of the process, but in a well-established cavitating flow regime. The test presented in column B considers bigger particles, submitted to a great number of cycles in a microreactor where the inception of cavitation had just began. Of course, a great number of complementary runs will have to be considered later. The experiments presented here are the first steps to know whether or not graphene can be exfolied from a microflow under a moderate pressure drop.

SEM observations (Fig. 9) have confirmed the good homogeneity of the size of the graphite particles used (both 1 µm and 20 µm) which nevertheless can form aggregates.

A snapshot of the flow corresponding to the batch A is presented in Figure 10. It is a top view of the channel, the suspension is flowing from the right to the left side of the picture. Even if the solid volume fraction of the suspension is below 1%, the presence of the particles is clearly noticeable upstream and downstream the constriction. A rough estimation of the real time during which strong shearing and cavitation are effective is made as follows: at the maximum velocity, a particle travels over 1 mm length during ≈30 µs. If we consider that exfoliation is likely to occur only during that period, the 25 passes correspond to a total processing time of 1 ms. The same calculation was performed with the data of the batch B (Tab. 2). At the end of the process, the solutions were centrifuged for 45 min at 4000 rpm (A) and 1500 rpm (B) respectively. The supernatant from each solution was collected for a TEM analysis (Philips CM300).

Figure 11 exhibits sheets issue from the batch A (Fig. 11a), batch B after 380 passes (Fig. 11b) and batch B after 800 passes (Fig. 11c). Some small flakes (Fig. 11a) look like few layers graphene. Their size is too small to allow a

TABLE 2
Summary of the preliminary tests conducted on two batches of the graphite dispersions.

Batch	A	B
Graphite supplier	*Sky Spring Inc.*	*Sigma Aldrich*
Concentration	5 g/L + 0.1 g/L NaC	10 g/L + 0.2 g/L NaC
Average size of the particles	1 µm	20 µm
Height "H" of the channel	383 µm	371 µm
Height "h" of the gap	110 µm	132 µm
$P_{in} - P_{out}$	10 bar	5 bar
Flow rate	13 L/h	10.2 L/h
Maximum average velocity "u_0"	32.8 m/s	21.5 m/s
Cavitation number "σ"	0.18	0.43
Number of passes	25	380 and 800
Effective cavitating time lived by the particles	1 ms	20 ms and 42 ms
Centrifugation before TEM observation of the supernatant	4000 rpm – 45 min	1500 rpm – 45 min

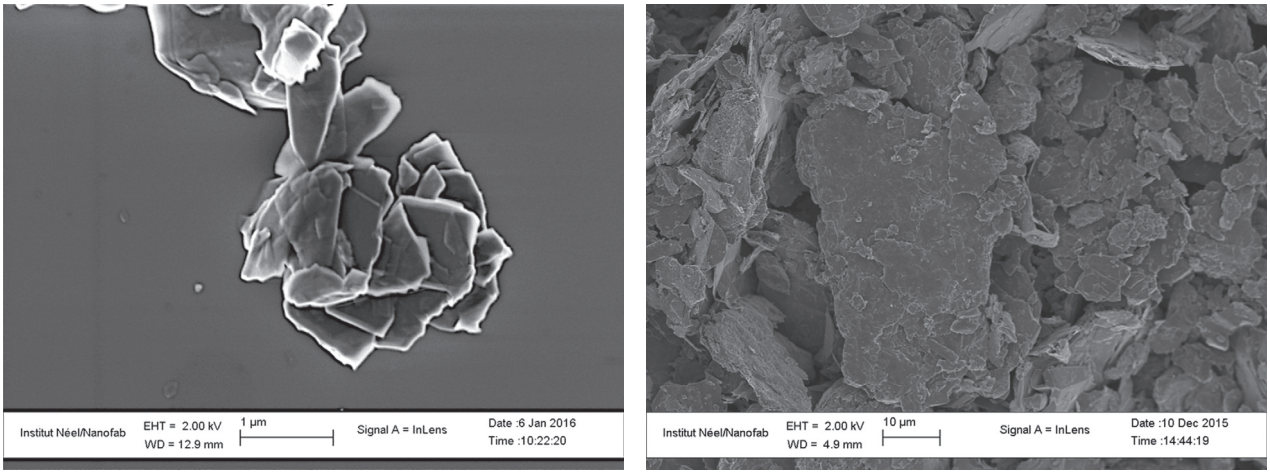

Figure 9

SEM observation of the two sorts of graphite microparticles (average size 1 µm and 20 µm) used as primary material for graphene exfoliation through cavitating microchannels.

diffraction analysis and to validate that they are graphene layers. As a matter of fact, the conjunction of initial small microparticles, low cavitation number and high centrifugation rate was not a conducive environment for the production of bigger flakes; shear rates and centrifugation rates control the flake size [25]: the highest, the lowest average size. Finest pictures have been recorded from the supernatant pipped from the batch B (Fig. 11b and 11c). Thin layers, whose lateral size is greater than 1 µm, are here clearly observable. Transmission electron diffraction patterns have confirmed the crystalline structure of the thin sheets. The number of passes does not seem to infer on the lateral size of the products issue from the batch B. Complementary experiments are needed, to draw final conclusions about the role of cavitation against the role of shear rate in LPE, and about the yield of the process.

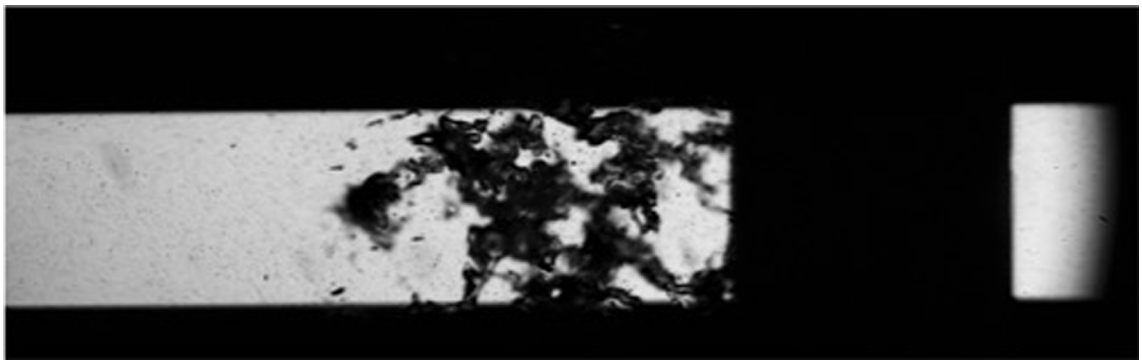

Figure 10

Optical snapshot of a cavitating microflow (top view) of a graphite suspension downstream a microstep. The fluid is flowing from the right to the left. The average velocity above the microstep is u_0 = 33 m/s.

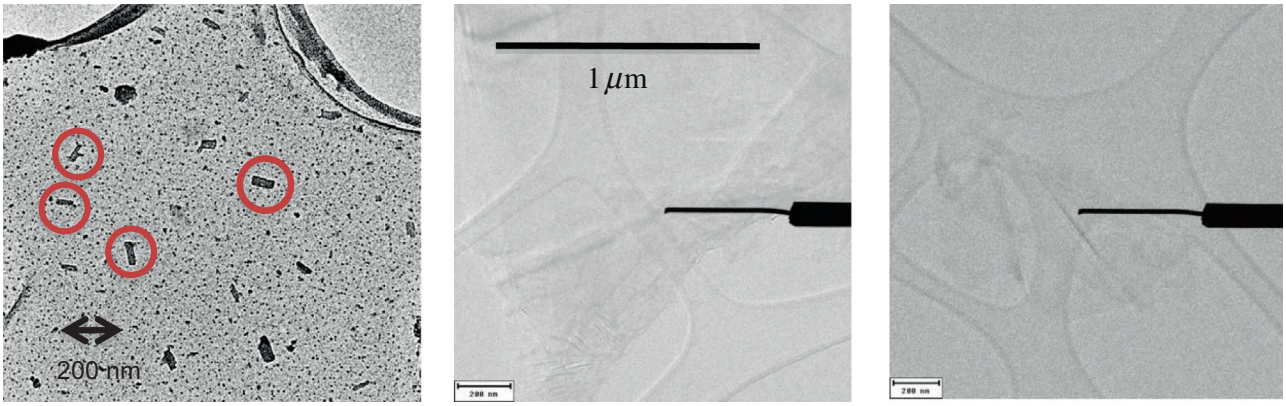

Figure 11

Flakes observed by Transmission Electron Microscopy (TEM) after processing. a) Batch A after 25 passes, the flakes are circled in red for a better understanding; b) and c) batch B after 380 and 800 passes respectively.

CONCLUSION

Hydrodynamic cavitation "on a chip" is a recent and powerful trend, that open new perspectives for the two-phase cavitating flows. A three dimensional thermal mapping of the liquid phase in cavitating flows has been performed for the first time. Thermal effects due to latent heat exchanges at the interfaces are likely to have an effect. Cavitation of viscous liquids or blends can also be monitored from a single liquid laminar flow regime; in that case, the two-phase flow exhibits quieter profiles than in a turbulent regime. Current projects are devoted to the application of the hydrodynamic cavitation "on a chip" for liquid phase exfoliation. These fluidic microsystems appear to provide a precious facility for interdisciplinary projects at the interfaces of physics, chemistry and engineering science.

ACKNOWLEDGMENTS

Part of this work was made possible through the French *ANR LUNAPROBE* Contract No. ANR 09-NANO-P057-36. This work has also been partially supported by the *LabEx Tec 21* (Investissements d'Avenir – Grant Agreement No. ANR-11-LABX-0030). The authors acknowledge helpful assistance of the technical staff of the Nanofab facilities from the *Neel Institute (CNRS)* of Grenoble.

REFERENCES

1 Suslick K.S., Flannigan D.J. (2007) Inside a collapsing bubble: Sonoluminescence and the conditions during cavitation, *Annu. Rev. Phys. Chem.* **59**, 659-683.

2 Mishra C., Peles Y. (2005) Flow visualization of cavitating flows through a rectangular slot micro-orifice ingrained in a microchannel, *Phys. Fluids* **17**, 113602.

3 Mishra C., Peles Y. (2005) Cavitation in flow through a micro-orifice inside a silicon microchannel, *Phys. Fluids* **17**, 013601.

4 Fernandez Rivas D., Prosperetti A., Zijlstra A.G., Lohse D., Gardeniers H.J.G.E. (2010) Efficient sonochemistry through microbubbles generated with micromachined surfaces, *Angew. Chem. Int. Ed.* **49**, 9699-9701.

5 Tandiono, Ohl S.-W., Ow D.S.W., Klaseboer E., Wong V.V., Dumke R., Ohl C.-D. (2011) Sonochemistry and sonoluminescence in microfluidics, *Proc. Nat. Acad. Sci. USA* **108**, 5996-5998.

6 Rooze J., André M., van der Gulik G.-J.S., Fernandez-Rivas D., Gardeniers J.G.E., Rebrov E.V., Schouten J.C., Keurentjes J.T.F. (2012) Hydrodynamic cavitation in micro channels with channel sizes of 100 and 750 micrometers, *Microfluid Nanofluid* **12**, 499-508.

7 Medrano M., Zermatten P.J., Pellone C., Franc J.P., Ayela F. (2011) Hydrodynamic cavitation in microsystems. I. Experiments with deionized water and nanofluids, *Phys. Fluids* **23**, 127103.

8 Nguyen N.T., Wereley S.T. (2002) *Fundamentals and applications of microfluidics*, Artech House Inc., Norwood, Massachusetts, USA.

9 Medrano M., Pellone C., Zermatten P.-J., Ayela F. (2012) Hydrodynamic cavitation in microsystems part II: Simulation and optical observations, *Phys. Fluids* **24**, 047101.

10 Zhu J., Zhao D., Xu L., Zhang X. (2016) Interactions of vortices, thermal effects and cavitation in liquid hydrogen cavitating flows, *Int. J. Hydrogen Energy* **41**, 614-631.

11 He Z., Zhong W., Wang Q., Jiang Z., Shao Z. (2013) Effect of nozzle geometrical and dynamic factors on cavitating and turbulent flow in a diesel multi-hole injector nozzle, *Int. J. Therm. Sci.* **70**, 132-143.

12 Serras-Pereira J., van Romunde Z., Aleiferis P.G., Richardson D., Wallace S., Cracknell R.F. (2010) Cavitation, primary break-up and flash boiling of gasoline, *iso*-octane and *n*-pentane with a real-size optical direct-injection nozzle, *Fuel* **89**, 2592-2607.

13 Ayela F., Medrano-Muñoz M., Amans D., Dujardin C., Brichart T., Martini M., Tillement O., Ledoux G. (2013) Experimental evidence of temperature gradients in cavitating microflows seeded with thermosensitive nanoprobes, *Phys. Rev. E: Stat. Phys., Plasmas, Fluids* **88**, 043016.

14 Ayela F., Colombet D., Ledoux G., Tillement O. (2015) Thermal investigation of cavitating flows through microchannels, with the help of fluorescent nanoprobes, *Houille Blanche – Revue internationale de l'eau* **1**, 102-108.

15 Vijayakumar T., Thundil Karuppa Raj R., Nanthagopal K. (2011) Effect of the injection pressure on the internal flow characteristics for diethyl and dimethyl ether and diesel fuel injectors, *Therm. Sci.* **15**, 4, 1123-1130.

16 Polat S. (2016) An experimental study on combustion, engine performance and exhaust emissions in a HCCI engine fuelled with diethyl ether-ethanol fuel blends, *Fuel Process. Technol.* **143**, 140-150.

17 Mossaz S., Colombet D., Ayela F. (2017) Hydrodynamic cavitation of binary liquid mixtures in laminar and turbulent flow regimes, *Exp. Therm. Fluid Sci.* **80**, 337-347.

18 Singh R., Peles Y. (2009) The effects of fluid properties on cavitation in a micro domain, *J. Micromech. Microeng.* **19**, 25009.

19 Novoselov K.S., Geim A.K., Morozov S.V., Jiang D., Zhang Y., Dubonos S.V., Grigorieva I.V., Firsov A.A. (2004) Electric field effect in atomically thin carbon films, *Science* **306**, 5696, 666-669.

20 Butler S.Z., Hollen S.M., Cao L., Cui Y., Gupta J.A., Gutiérrez H.R., Heinz T.F., Hong S.S., Huang J., Ismach A.F., Johnston-Halperin E., Kuno M., Plashnitsa V.V., Robinson R.D., Ruoff R.S., Salahuddin S., Shan J., Shi L., Spencer M.G., Terrones M., Windl W., Goldberger J.E. (2013) Progress, challenges, and opportunities in two-dimensional materials beyond graphene, *ACS Nano* **7**, 4, 2898-2926.

21 Geim A.K., Grigorieva I.V. (2013) Van der Waals heterostructures, *Nature* **499**, 419-425.

22 Yi M., Shen Z. (2015) A review on mechanical exfoliation for the scalable production of graphene, *J. Mater. Chem. A* **3**, 11700-11715.

23 Arao Y., Mizuno Y., Araki K., Kubouchi M. (2016) Mass production of high-aspect ratio few-layer-graphene by high-speed laminar flow, *Carbon* **102**, 330-338.

24 Ciesielski A., Samori P. (2014) Graphene *via* sonication assisted liquid-phase exfoliation, *Chem. Soc. Rev.* **43**, 381-398.

25 Paton K.R., Varrla E., Backes C., Smith R.J., Khan U., O'Neill A., Boland C., Lotya M., Istrate O.M., King P., Higgins T., Barwich S., May P., Puczkarski P., Ahmed I., Moebius M., Petterson H., Long E., Coelho J., O'Brien S.E., McGuire E.K., Mendoza Sanchez B., Duesberg G.S., McEvoy N., Pennycook T.J., Downing C., Crossley A., Nicolosi V., Coleman J.N. (2014) Scalable production of large quantities of defect-free few-layer graphene by shear exfoliation in liquids, *Nat. Mater.* **13**, 624-630.

26 Shen Z., Li J., Yi M., Zhang X., Ma S. (2011) Preparation of graphene by jet cavitation, *Nanotechnology* **22**, 365306.

27 Nacken T.J., Damm C., Walter J., Rüger A., Peukert W. (2015) Delamination of graphite in a high pressure homogenizer, *RSC Adv.* **5**, 57328.

28 Chevalier J., Ayela F. (2008) Microfluidic on chip viscometers, *Rev. Sci. Instrum.* **79**, 7, 076102.

Manuscript submitted in September 2016
Manuscript accepted in April 2017
Published online in July 2017

Cite this article as: F. Ayela, W. Cherief, D. Colombet, G. Ledoux, M. Martini, S. Mossaz, D. Podbevsek, X. Qiu and O. Tillement (2017). Hydrodynamic Cavitation through "Labs on a Chip": From Fundamentals to Applications, *Oil Gas Sci. Technol* **72**, 19.